Journal of Materials Chemistry A

Accepted Manuscript

ROYAL SOCIETY OF CHEMISTRY

www.rsc.org/materialsA

Triethanolamine Functionalized Graphene-Based Composite for High Performance Supercapacitors

Bo Song,[a,b] *Chelsea Sizemore,*[a] *Liyi Li,*[a] *Xiaogu Huang,*[a,c] *Ziyin Lin,*[a,b] *Kyoung-sik Moon*[a,]* *and Ching-Ping Wong*[a,d,]*

[a]School of Materials Science and Engineering, Georgia Institute of Technology, 771 Ferst Drive, Atlanta, GA 30332, United States,

[b]School of Chemistry and Biochemistry, Georgia Institute of Technology, 901 Atlantic Drive, Atlanta, GA 30332, United States,

[c]School of Physics and Optoelectronic Engineering, Nanjing University of Information Science & Technology, Nanjing, 210044, China,

[d]Department of Electronic Engineering, The Chinese University of Hong Kong, Shanti, Hong Kong

*E-mail: cpwong@cuhk.edu.hk; ks.moon@mse.gatech.edu

Abstract

In this work, a graphene-based nanocomposite was prepared for high-capacity supercapacitor electrode using triethanolamine (TEA) as inter-layer spacer via a controlled hydrothermal process. The chemical functionalization of the molecular spacer onto the reduced graphene oxide (rGO) surface considerably increased the specific surface area and generated a 3D porous graphene network for efficient ionic diffusion and transport. In addition, the formation of oxygen-containing groups in the composite could effectively tune the surface chemistry, making the electrolyte ions more accessible to electrode nanostructure. The unique compositional and structural features of the TEA/rGO were confirmed by several techniques, including TGA, FTIR, XPS, XRD and BET measurement. The as-fabricated electrode exhibited a superior capacitance of 211 F/g in a two-electrode configuration with excellent rate performance, low charge transfer resistance and outstanding cycling stability (91.7% of initial capacitance retained after 10,000 cycles). Furthermore, a maximum energy density of 25.7 Wh/kg was achieved in the organic electrolyte at 2.5 V potential range. These impressive electrochemical characteristics of TEA/rGO composite make it highly promising for high performance energy storage applications.

Introduction

Supercapacitors with high power densities and long cycle life have attracted great research interest for energy storage systems.[1,2] Generally, supercapacitors store energy via charge accumulation at electrode/electrolyte interface (electrical double layer capacitors (EDLCs)) or reversible Faradic reactions (pseudocapacitors) in the presence of conductive polymers or metal oxides.[3,4] Recently, graphene has been regarded as a promising electrode material in EDLCs owning to its high electrical conductivity, large specific surface area (SSA), and open-porous nanostructure.[5-7] Theoretically, the SSA of fully exfoliated graphene sheets can reach as high as 2600m^2/g, which provides electrical double layer (EDL) capacitance up to 550 F/g.[8,9] Currently, a variety of strategies have been developed to produce graphene, including chemical vapor deposition (CVD), carbonization of biomass, and chemical or thermal reduction of graphene oxide (GO) to reduced graphene oxide (rGO).[10-16] In addition to these methods, hydrothermal processing is considered to be a simple, low energy-consuming and environmentally friendly approach for large-scale production of graphene because it typically operates at low temperatures (<200°C) and requires no hazardous reducing agents.[13,17] In addition, the hydrothermal treatment can achieve easy control of the surface morphology and functionalities of the graphene nanostructure by adjusting the reaction time and temperature.[18]

Despite the strength of hydrothermal method, it is inevitable that graphene sheets will restack into multiple layers during the reduction process. The agglomeration of the graphene sheets significantly deteriorates the effective surface area and charge storage capacity compared with exfoliated monolayer graphene.[19,20] Therefore, various types of interlayer "spacers" have been introduced to enlarge the interlayer spacing of graphene sheets and ensure the utilization of large surface area; some examples of spacers include metal oxides, conductive polymers and carbon nanomaterials.[21-26] For example, Cheng et al. reported the anchoring of RuO_2 between graphene sheets as interlayer spacers.[27] Hollow polypyrrole nanotubes (PNTs) are also incorporated into graphene aerogel and the modified graphene composite showed specific capacitance up to 253 F/g.[28] These pseudocapacitive spacers can contribute to the overall capacitance of the electrode materials, but the long-term structural and cycling stability of the pseudocapacitive components remains an issue. In addition, few-layer graphene is obtained by assembling CNTs, carbon and SiO_2 nanospheres on graphene sheets with porous and hierarchical nanostructures.[29-31] However, the self-assembly process driven by π-π or electrostatic interactions is not strong enough to achieve uniform and consistent intercalation of spacers.[28,30] In this sense, molecular-scale organic spacers that rely on chemical bonds, rather than intermolecular interactions, can be used to effectively avoid the collapsing of 3D graphene architecture with good control of surface chemistry. The surface chemistry plays a critical role in tuning the wettability of the surface and the effect of reversible redox reactions. For the organic spacers, researchers have reported many amine molecules to be grafted on graphene as interlayer spacer.[32-34] As an alternative approach, alcohol-based spacers with hydroxyl groups have also been chemically bonded to graphene with increased surface area and electrolyte wetting for energy storage.[25]

Herein we report on a facile hydrothermal approach to prepare triethanolamine (TEA) functionalized rGO (TEA/rGO) composite as high performance supercapacitor electrodes. As a molecular spacer, TEA can be grafted on GO surface to reduce the aggregation of graphene and greatly increase the interlayer spacing. In addition, incorporating tri-functional TEA enables the formation of more chemical bonds between adjacent GO layers, thus producing a more stabilized 3D graphene structure with enhanced surface area. Furthermore, the chemical modification by TEA during hydrothermal process can tune the surface chemistry of graphene. The large amount of oxygen-containing groups considerably improves the wettability of aqueous electrolyte ions onto the electrode, resulting in more ion access to the electrode surface and improved charge storage capability. Due to the synergistic effect of enlarged ion accessible surface area, robust 3D nanostructure and optimized surface energy, our TEA/rGO electrode exhibits a high specific capacitance of 211 F/g with excellent rate performance and cycling stability.

Experimental

Preparation of TEA/rGO electrode materials

Graphene oxide (GO) was prepared by modified Hummers' method, and the viscous triethanolamine liquid was diluted 10 times by deionized (DI) water and used as stock solution. To prepare TEA/rGO samples, 30 mg GO was dispersed in 60 mL DI water and sonicated for 1 h. After that, 1.5 mL of TEA stock solution was slowly added to the GO dispersion and vigorously stirred for 30 min to form a homogenous dispersion. The mixed dispersion was transferred to a 100 mL Teflon-lined autoclave for hydrothermal reaction at 105°C for 5 h and 180°C for 10 h. The resultant precipitate was filtered, washed with DI water and ethanol repeatedly to remove the unreacted TEA, and dried at 55°C overnight. rGO control sample was prepared by dispersing 30 mg of GO in 60 mL of DI water and processed at the same condition as TEA/rGO composite.

Characterizations

A Hitachi SU8010 field-emission scanning electron microscopy (SEM), a Joel 100CX transmission electron microscopy (TEM) and a Veeco Dimension Edge atomic force microscope (AFM) were used to characterize the morphology of the TEA/rGO. Thermogravimetric analysis (TGA) was taken on a TGA-2050 analyzer (TA Instruments Co). The X-ray diffraction data was obtained by X'Pert Alpha-1 diffractometer, using Cu Kα radiation (45 kV and 40 mA). Contact angle measurements with water droplet were performed in room temperature with a Rame-Hart goniometer. The X-ray photoelectron spectroscopy (XPS) was collected on Thermo K-Alpha XPS, and Fourier Transform Infrared Spectroscopy (FTIR) was recorded on a Magna IR 560 (Nicolet) spectrophotometer. Raman spectra was obtained from LabRAM ARAMIS, HORIBA JOBIN YVON with 532 nm laser.

Electrochemical characterizations

The free-standing thin film electrodes were prepared by mixing active materials (90 wt%) with polytetrafluoroethylene (PTFE, 10 wt%) binder in DI water. The binder used (MTI Inc.) is an aqueous dispersion liquid that is stabilized by non-ionic surfactant (3~4%) with solid PTFE content up to 60 w% (+/-2%). After homogeneous mixing, the resultant paste was rolled to a uniform film with average thickness around 80 μm and dried at 55°C for 12 h before use. The electrochemical performance of the thin film electrodes (average mass loading of (1±0.2) mg with 6 mm in diameter for each electrode) were tested in a symmetric two-electrode system in coin cells using both 1 M H_2SO_4 and 1 M tetraethylammonium tetrafluoroborate in acetronitrile ($TEABF_4$/AN) as electrolytes. Cyclic voltammetry (CV), galvanostatic charge/discharge (CD), and electrochemical impedance spectroscopy (EIS) were all carried out a Versastat 2-channel system (Princeton Applied Research). The specific capacitance was calculated from both CV ($C_{sc} = \frac{2\int IdV}{vmV}$) and CD ($C_{sc} = \frac{4It}{mV}$) profiles, where I is the current, V is the potential range, v is the scan rates, m is the total mass of two electrodes, and t is the discharge time. The energy and power density were also determined based on the following formula: $E = C_{sc}V^2/8$, $P = E/t$, where C_{sc} is the specific capacitance, V is the applied voltage, and t is the discharge time.

Results and discussion

The schematic illustration of the chemical reaction and the corresponding 3D graphene-based architecture was shown in Scheme 1. Upon ultrasonication, the GO and TEA mixture could form a stable and homogeneous dispersion, as shown in Fig. S1. At 105°C, TEA molecule can be grafted on graphene surface to exfoliate the stacked graphene sheets. The hydrothermal treatment at 180°C serves to ensure more complete reduction of GO. The enlarged surface area, together with the stronger electrolyte affinity to graphene surface at the presence of hydrophilic TEA spacer, brings a synergistic effect to facilitate the charge diffusion through graphene layers. To investigate the nanostructure of the TEA/rGO, a series of morphological studies are presented. Fig. 1(a) shows the SEM image of the TEA/rGO with typical sheets-like graphene morphology with well-exfoliated thin layer features. The TEM image (Fig. 1b) reveals the wrinkled form of functionalized rGO with no obvious aggregation. Low contrast of rGO sheets compared to non-sample region and clear edges indicate the small thickness of the nanostructure. Fig. 1c clearly presents an individual TEA/rGO flake with slightly wrinkled surfaces. The average thickness of the flake is determined to be ~ 1.96 nm from the corresponding height profile (Fig. 1d). The AFM image of a single layer GO flake with an average depth of 1.10 nm is shown in Fig. S2 as a comparison. In the absence of layer-by-layer aggregation, we believe that the increased thickness of the TEA/rGO nanostructure is mainly attributed to the presence of TEA molecules, either intercalated in-between graphene layers or grafted on outer graphene surfaces.

The chemical and compositional characterizations of TEA modified rGO are measured by FTIR, DSC, Raman and XPS. FTIR was used to elucidate the chemical bonds between GO and TEA. As shown in Fig.2a, the FTIR spectrum of GO exhibits a series of functional groups, including hydroxyl (-OH, 3400 cm^{-1}), carbonyl (C=O, 1735 cm^{-1}), epoxy (C-O-C, 1260 cm^{-1}) and alkoxyl groups (C-O, 1100cm^{-1}). The intensity of carbonyl and alkoxyl bands decrease significantly after hydrothermal reduction. Upon functionalization, TEA/rGO presents two strong bands at 1260

cm^{-1} and 1066 cm^{-1}, which are ascribed to the epoxy and alkoxyl groups respectively. These enhanced C-O characteristics suggests an obvious covalent linkage of TEA onto graphene sheets. Furthermore, two emerging peaks at 1468 and 715 cm^{-1} ($–CH_2$ bending modes), together with the intensified peaks at 2925 and 2854 cm^{-1} (stretching modes of $–CH_2$ units), all confirms the existence of the TEA molecules in the graphene structure. The FTIR spectrum of pure TEA is also presented in Fig. S3 as a reference. Fig. 2b shows DSC profiles of GO/TEA mixture, which is used to monitor the in-situ reaction process. From 105°C to 173°C, a prominent exothermic peak was observed with a calculated enthalpy of 975 J/g, which provides an evidence for the exothermic reactions between GO and TEA. It is believed that the ring opening of epoxide groups or the condensation of hydroxyl groups are mostly likely to occur at the temperature range with strong exothermic features. The resulting composite with higher content of C-O functionalities is also confirmed by FTIR. The reaction onset temperature, 105°C, is used as the first step temperature for the molecular grafting. This low-temperature treatment can maximize the degree of chemical reactions before GO is further reduced at 180°C. Raman spectroscopy is used to illustrate the graphitic crystalline structure. As shown in Fig. 2c, the D band at 1340 cm^{-1} represents structural defects while the G band 1590 cm^{-1} corresponds to the ordered sp^2 hybridized graphene network.[35] It was found that I_D/I_G ratio was 0.97 for GO, increased slightly to 1.09 for rGO and 1.13 for TEA/rGO. The small increase of the I_D/I_G ratio between rGO and TEA/rGO is due to the TEA incorporation, in which the grafting of TEA molecule on graphene surface replaces some of the sp^2 carbon sites and generates more sp^3 carbon forms. In addition, the 2D peak was observed at around 2700 cm^{-1} after GO reduction, which is caused by the second order vibration of two phonons with opposite wavevectors.[36] For TEA/RGO composite, the pronounced intensity of the 2D peak relative to rGO indicates the improved exfoliation of graphene sheets to fewer layers upon molecular functionalization.[37]

XPS was used to provide further insight on the TEA/rGO nanostructure. From the survey spectrum (Fig. 2d), the N content is quantified to be ~2.05%, which provides an estimated percentage of 20.5% of TEA spacer in the composite (atomic ratios C:O:N=6:1:3). The liquid-state TEA is highly miscible with water; only the covalently bonded molecules can remain in the composite after repeated washing processes. Figure. 2d (inset) shows the high resolution C1s spectrum of the composite. Peak deconvolution reveals that there is 69.6% C=C, 16.1% C-O, 8.4% C-N & C=O, and 5.9% O-C=O.[33,38] Among the oxygen-containing groups, the largest fraction of C-O bonds, further indicates covalent linkage between TEA and graphene, as complementary to FTIR.[18] The survey XPS spectrum of rGO is shown in Fig. S4. It can be seen that the O content increases from 9.95% to 15.75% via upon TEA modification. The surface functionalities, specifically O-containing groups, can effectively tune the surface energy of the materials. In particular, the wettability is important for electrochemical performance since good wetting properties facilitate the ion adsorption at the inner pores of electrode. The contact angle measurements were performed to investigate the wettability of the TEA/rGO electrode. As shown in Fig. S5a, the contact angle of 78.9±2.0° is obtained with a water droplet on a TEA/rGO film, whereas the contact angle for the rGO control sample is determined to be 107.4±1.0° (Fig.

S5b). The hydrophilic nature of the modified electrode is mainly attributed to the sufficient amount of C-O groups in the composite.

TGA curves of GO, rGO, TEA/rGO and pristine TEA in air are shown in Fig. 3a to further investigate the thermal stability. In accordance with previous literature, GO has a dramatic weight loss between 150°C to 250°C due to the removal of liable oxygen-containing groups.[39] Above 550°C, the sp^2 hybridized carbon network in GO and rGO became completely degraded. The organic TEA spacer and TEA-rGO mixture without any chemical reactions are thermally unstable and decomposed at around 150°C (Fig. S6). In contrast, the TEA-functionalized rGO showed higher degradation onset temperature at ~220°C, which indicates the improved thermal stability of the composite via chemical bonding. The gradual weight (~ 15%) loss from 230°C to 500°C arises from the slow decomposition of grafted TEA on rGO. Similarly, the TEA/rGO composite went through thorough decomposition at ~515°C.

Fig. 3b shows the XRD patterns of GO, rGO and TEA/rGO. GO displays a characteristic diffraction peak at 9.9°, corresponding to an interlayer spacing of 0.90 nm. Upon the hydrothermal reduction, the loss of considerable oxygen-containing groups occurs, and rGO becomes restacked, which reduces the interlayer spacing (~0.35 nm) and accessible surface areas for electrolyte ions. Upon the grafting of TEA, a new diffraction peak was observed at 5.1°, which is much lower than that of GO (9.9 °). The broadened interlayer spacing (1.75 nm) was attributed to the intercalation of TEA as molecular spacer, which serves to reduce the agglomeration of curved graphene sheets to some extent. Particularly, TEA molecule with highly branched structure, is more likely to form a 3D graphene architecture with stabilized interlayer spacing and enhanced surface area. Moreover, the interlayer thickness calculated by Bragg's law is consistent with that measured by AFM. In conjugation with XRD, N_2 adsorption-desorption isotherms was used to examine the spacing effect of TEA/rGO sample. As shown in Fig. 4a, our TEA/rGO composite displays a type-IV isotherm with SSA up to 527.8 m^2/g, which shows a three-fold improvement compared with rGO (189.8 m^2/g, Fig. S7). The dramatic raise in the adsorption curve at low relative pressure indicates a large content of micropores, while the clear hysteresis loop at the relative pressure of (0.4~0.85) corresponds to the capillary condensation of mesopores between graphene layers.[20] Fig. 4b presents the pore size distribution plots of TEA/rGO with an average pore width of 2.96 nm. The TEA/rGO composite containing different pore sizes ensures the efficient charge transfer through mesopores and provides the sufficient surface area for charge storage within micropores.

The electrochemical performance of the TEA/rGO films was measured by cyclic voltammetry (CV) using a two-electrode symmetrical coin cell in 1 M H_2SO_4 electrolyte. Fig. 5a shows the CV plots with various scan rates from 2 to 200 mV/s. The symmetric and near-rectangular curves at different scan rates indicate the efficient charge transfer through the porous structure of electrode materials. The absence of obvious anodic/cathodic peaks in CV curves further implies that the oxygen-containing functional groups on graphene surface have been largely removed during TEA functionalization and hydrothermal reduction processes. Therefore, EDL effect

contributes predominantly to the capacitance as more charges can be stored at the enlarged interlayer space between graphene sheets .The rate-dependent capacitance results calculated from CV curves is shown in Fig. 5b. It can be seen that the maximum specific capacitance reaches as high as 210 F/g at 2 mV/s, which can be attributed to the synergistic effect of large ionic accessible surface area and good wettability of the electrolyte, as discussed above. As the increase of scan rates, the specific capacitance decreases to 190 F/g at 10 mV/s and 166 F/g at 50 mV/s. Importantly, the specific capacitance is kept as high as 156 and 143 F/g at 100 and 200 mV/s, which retained 74.3% and 68.1% of the capacitance from the capacitance value at 2 mV/s, respectively. This excellent rate performance further signifies a strong EDL feature of the TEA-grafted graphene structure. The capability of the materials to operate at high power conditions offers possibility for electronic devices that requires ultrafast charge/discharge handling. The TEA/rGO thin film electrodes were also tested using organic electrolytes (1 M TEA/BF_4) in two-electrode configuration. Fig. 5c shows the CV curves of TEA/rGO from 10 to 200 mV/s with applied voltage up to 2.5V. As shown in the rate-performance plot (Fig. S8a), the highest specific capacitance of 118 F/g was achieved for TEA/rGO at 10mV/s. The enhanced interlayer spacing of TEA/rGO can facilitate the bulkier-sized electrolyte ions to penetrate through the inner pores, thus resulting in more charge accumulation at the electrode/electrolyte interface for energy storage. The CV curves and rate-dependent capacitance plots of rGO control sample in both aqueous and organic electrolytes are shown in Fig. S9 as the benchmark. Generally, graphene-based composite decorated by conductive polymers or metal oxide shows a high energy density, but the relatively slow charge/discharge rates and the poor cycling stability limit their usage. As for the TEA/rGO composite that predominantly relies on EDL energy storage, the highest energy density is determined to be 25.7 Wh/kg at 2.5 V in organic electrolyte. The compatibility of the electrode materials in organic electrolyte provides the feasibility for high energy-density applications.

Fig. 5d and Fig. S10a show the galvanostatic charge/discharge (CD) profiles at different current densities. The symmetric and linear lines of the charging/discharging curves indicate capacitive features of the charge propagation in a reversible manner. At all current densities, the small voltage drop implies a small series resistance. From the CD curves, the specific capacitances are calculated to be ~200 F/g, 183 F/g, 152 F/g and 144 F/g at current densities of 0.2, 1, 5 and 10 A/g, respectively. The decrease of specific capacitance with increasing current densities is attributed to limited ionic diffusion at fast charge/discharge rates. It has been found that the specific capacitance was in accordance with the values calculated from CV profiles at corresponding discharge times, as shown in Fig. S10b. In 1M H_2SO_4 electrolyte, the maximum power density of 5.1 kW/kg was obtained at an energy density of 5.0 Wh/kg. Cycling stability of the TEA/rGO electrodes were investigated at current densities of 2 A/g. It can be seen from Fig. 5e that ~91.7% of capacitance is retained after 10,000 cycling tests. In organic electrolyte, ~ 91.4% of the capacitance is also reversibly maintained after 10,000 cycles, as shown in Fig. S8(b). The outstanding cycling durability, together with excellent rate performance and electrolyte wettability, demonstrates the unique nanostructure of TEA/rGO composite for charge storage,

which shows apparent advantages over other types of molecular spacer functionalized graphene materials. [40-43]

Electrochemical impedance spectroscopy (EIS) was used to study the resistive properties and the ionic diffusion kinetics of the electrode film in 1 M H_2SO_4. Fig. 5f shows the Nyquist plots at a frequency range from 100 kHz to 0.01 Hz, with a magnified view at high frequency in the inset. The near-perpendicular line at the mid-to-low frequency regions indicates an almost ideal capacitive behavior with fast ionic transfer. In the Nyquist plot, the first intersection point on the real axis is defined as the series resistance (R_s), which includes electrolyte resistance, electrode resistance, and interfacial resistance between electrode and current collector.[44] The small R_s value (0.38 Ω) indicates the excellent electrical conductivity provided by the electrode material. By extrapolating the second intersection point of the semicircle on real axis, the charge transfer (R_{ct}) resistance is obtained. This low value R_{ct} (1.37 Ω) represents the small interfacial resistance between electrode and electrolyte, which further demonstrates the superior wettability of the electrodes by introducing more O-containing functionalities on graphene surface. The TEA/rGO electrodes in organic electrolyte also show near perpendicular lines at low frequency (Fig. S8c), and this further proves the good ionic diffusion behavior.

Conclusions

In summary, we have successfully fabricated the TEA/rGO composite as supercapacitor electrode by a simple hydrothermal process at a low temperature. As an interlayer spacer, the tri-functional TEA molecule bonded to graphene surface can effectively suppress the graphene agglomeration and create a stabilized 3D graphene architecture. The enlarged surface area with desirable pore sizes significantly promotes the diffusion and anchoring of electrolyte ions. In addition, the functionalization of TEA at controlled reaction condition can reserve large quantity of oxygen-containing functionalities, which dramatically enhances the ion accessibility to the electrode. Due to these unique structural and chemical attributes, the TEA/rGO exhibits a high specific capacitance of 211 F/g with 91.7% capacitance maintained after 10,000 cycling tests in 1 M H_2SO_4. In addition, TEA/rGO electrode also shows a remarkable charge storage performance in organic electrolyte with an enhanced energy density of 25.7 Wh/kg at 2.5 V. Moreover, this work offers a universal synthetic strategy for the rational design of novel molecular spacer-decorated graphene nanostructure for energy storage materials.

Acknowledgement

This research work was supported by Advanced Research Project Agency-Energy Program # DE-AR0000303.

Footnotes

Electronic supplementary information (ESI) available: digital images of TEA/GO dispersion, AFM image of GO, FTIR spectrum of TEA, XPS spectrum of rGO, contact angle measurement

images, TGA curves of TEA, N_2 adsorption/desorption isotherm, and electrochemical data comparison.

References

(1) J. R. Miller, P. Simon, *Science,* 2008, **321**, 651-652.
(2) G. Wang, L. Zhang, J. Zhang, *Chem. Soc. Rev.,* 2012, **41**, 797-828.
(3) C. Liu, Z. Yu, D. Neff, A. Zhamu, B. Z. Jang, *Nano Lett.* 2010, **10**, 4863-4868.
(4) Y. Zhang, H. Feng, X. Wu, L. Wang, A. Zhang, T. Xia, H. Dong, X. Li, L. Zhang, A review. *Int. J. Hydrogen Energy,* 2009, **34**, 4889-4899.
(5) A.K. Geim, *Science,* 2009, **324**, 1530-1534.
(6) Y. Zhu, S. Murali, M. D. Stoller, K. Ganesh, W. Cai, P. J. Ferreira, A. Pirkle, R. M. Wallace, K. A. Cychosz, M. Thommes, D. Su, E. A. Stach, R. S. Ruoff, *Science,* 2011, **332**, 1537-1541.
(7) Z. Li, B. Song, Z. Wu, Z. Lin, Y. Yao, K. S. Moon, C. P. Wong, *Nano Energy,* 2015, **11**, 711-718.
(8) M. D. Stoller, S. Park, Y. Zhu, J. An, R. S. Ruoff, . Graphene-based ultracapacitors. *Nano Lett.,* 2008, **8**, 3498-3502.
(9) Y. Wang, Z. Shi, Y. Huang, Y. Ma, C. Wang, M. Chen, Y. Chen, *J. Phys. Chem. C,* 2009, **113**, 13103-13107.
(10) Y. Zhu, S. Murali, W. Cai, X. Li, J. W. Suk, J. R. Potts, R. S. Ruoff, *Adv. Mater.,* 2010, **22**, 3906-3924.
(11) A. Reina, X. Jia, J. Ho, D. Nezich, H. Son, V. Bulovic, M. S. Dresselhaus, J. Kong, J. *Nano Lett.* 2008, **9**, 30-35.
(12) P. Hao, Z. Zhao, Y. Leng, J. Tian, Y. Sang, R. I. Boughton, C. P. Wong, H. Liu, B. Yang, *Nano Energy,* 2015, **15**, 9-23.
(13) H. Zhang, T. Kuila, N. H. Kim, D. S. Yu, J. H. Lee, *Carbon,* 2014, **69**, 66-78.
(14) Z. Wu, Z. Lin, L. Li, B. Song, K. S. Moon, S. L. Bai, C. P. Wong, *Nano Energy,* **2014**, *10*, 222-228.
(15) U. N. Maiti, J. Lim, K. E. Lee, W. J. Lee, S. O. Kim, *Adv. Mater.* 2014, **26**, 615-619.
(16) Z.Wu, L. Li, Z. Lin, B. Song, L. Li, K. S. Moon, C. P. Wong, S. L. Bai, *Scientific Reports,* 2015, **5**.
(17) Y. Xu, K. Sheng, C. Li, G. Shi, *ACS Nano,* 2010, **4**, 4324-4330.
(18) Z. Lin, Y. Liu, Y. Yao, O. J. Hildreth, Z. Li, K. Moon, C. P. Wong, *J. Phys. Chem. C,* 2011, **115**, 7120-7125.
(19) R. B. Rakhi, W. Chen, D. Cha, H. Alshareef,. *Adv. Energy Mater.,* 2012, **2**, 381-389.
(20) H. Zhang, K. Wang, X. Zhang, H. Lin, X. Sun, C. Li, Y. Ma, *J. Mater. Chem. A,* 2015, **3**, 11277-11286.
(21) J. Yan, Z. Fan, T. Wei, W. Qian, M. Zhang, F. Wei, *Carbon,* 2010, **48**, 3825-3833.
(22) X. C. Dong, H. Xu, X. W. Wang, Y. X. Huang, M. B. Chan-Park, H. Zhang, L. H. Wang, W. Huang, P. Chen, *ACS Nano,* 2012, **6**, 3206-3213.
(23) N. A. Kumar, H. J. Choi, Y. R. Shin, D. W. Chang, L. Dai, J. B. Baek, *ACS Nano,* 2012, **6**, 1715-1723.
(24) G. Wang, X. Sun, F. Lu, H. Sun, M. Yu, W. Jiang, C. Liu, J. Lian, *Small,* 2012, **8**, 452-459.

(25) Y. Yu, Y. Sun, C. Cao, S. Yang, H. Liu, P. Li, P. Huang, W. Song, *J. Mater. Chem. A,* 2014, **2**, 7706-7710.
(26) B. Song, L. Li, Z. Lin, Z. Wu, K. S. Moon, C. P. Wong, *Nano Energy,* 2015, **16**, 470-478.
(27) Z. S. Wu, D. W. Wang, W. Ren, J. Zhao, G. Zhou, F. Li, H. M. Cheng, *Adv. Funct.Mater.,* 2010, **20**, 3595-3602.
(28) S. Ye, J. Feng, *ACS Appl. Mater. Interfaces,* 2014, **6**, 9671-9679.
(29) Y. Wang, Y. Wu, Y. Huang, F. Zhang, X. Yang, Y. Ma, Y. Chen, *J. Phys. Chem. C,* 2011, **115**, 23192-23197.
(30) C. X. Guo, C. M. Li, *Energy Environ. Sci.,* 2011, **4**, 4504-4507.
(31) T. Li, N. Li, J. Liu, K. Cai, M. F. Foda, X. Lei, H. Han, *Nanoscale,* 2015, **7**, 659-669.
(32) Z. Liu, H. Zhou, Z. Huang, W. Wang, F. Zeng, Y. Kuang, *J. Mater. Chem. A,* 2013, **1**, 3454-3462.
(33) O. C. Compton, D. A. Dikin, K. W. Putz, L. C. Brinson, S. T. Nguyen, *Adv. Mater.,* 2010, **22**, 892-896.
(34) W. S. Hung, C. H. Tsou, M. De Guzman, Q. F. An, Y. L. Liu, Y. M. Zhang, C. C Hu, K. R. Lee, J. Y. Lai, Chem. Mater., 2014, **26**, 2983-2990.
(35) A. C. Ferrari, J. Robertson, *Phys. Rev. B,* 2000, **61**, 14095.
(36) M. Iqbal, A. K. Singh, M. Iqbal, J. Eom, J. Phys.: Condens. Matter, 2012, 24, 335301.
(37) S. Niyogi, E. Bekyarova, M. E. Itkis, H. Zhang, K. Shepperd, J. Hicks, M. Sprinkle, C. Berger, C. N. Lau, W. A. Deheer, Nano Lett., 2010, **10**, 4061-4066.
(38) Z. Lin, G. Waller, Y. Liu, M. Liu, C. P. Wong, Adv. Energy Mater., 2012, ***2***, 884-888.
(39) M. J. McAllister, J. L. Li, D. H. Adamson, H. C. Schniepp, A. A. Abdala, J. Liu, J.; M. Herrera-Alonso, D. L. Milius, R. Car, R. K. Prud'homme, *Chem. Mater.,* 2007, **19**, 4396-4404.
(40) J. An, J. Liu, Y. Zhou, H. Zhao, Y. Ma, M. Li, M. Yu, S. Li, J. Phys. Chem. C, 2012, **116**, 19699-19708.
(41) X. Liu, P. Shang, Y. Zhang, X. Wang, Z. Fan, B. Wang, Y. Zheng, J. Mater. Chem. A, 2014, **2**, 15273-15278.
(42) H. Li, Y. Wang, Y. Shi, J. Li, L. He, H. Y. Yang, RSC Adv., 2013, **3**, 14954-14959.
(43) H. N. Tien, N. T. M. Hien, E. S. Oh, J. Chung, E. J. Kim, W. M. Choi, B. S. Kong, S. H. Hur, J. Mater. Chem. A, 2013, **1**, 208-211.
(44) X. Li, J. Rong, B. Wei, *ACS Nano,* 2010, **4**, 6039-6049.

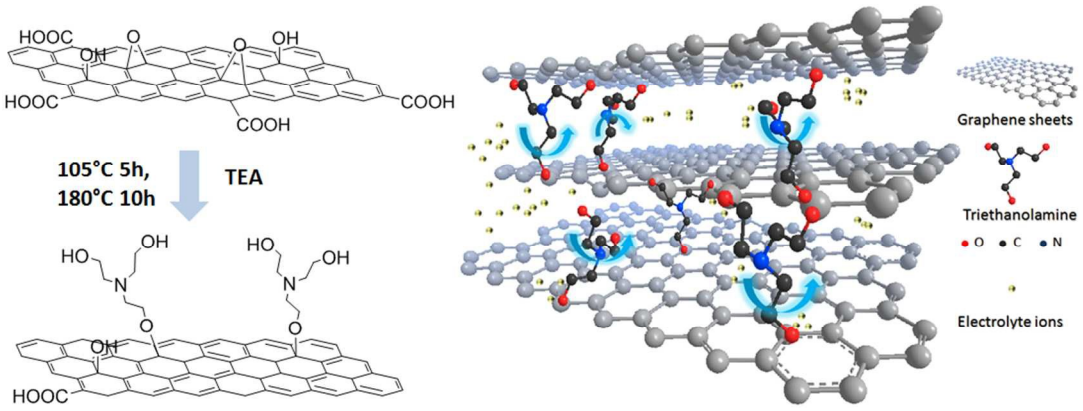

Scheme 1. Schematics of the chemical reaction between TEA and GO (left) and the as-formed 3D TEA/rGO nanostructure with charge transfer characteristics (right); the residue oxygen-containing groups on graphene sheets are omitted for clarity (right).

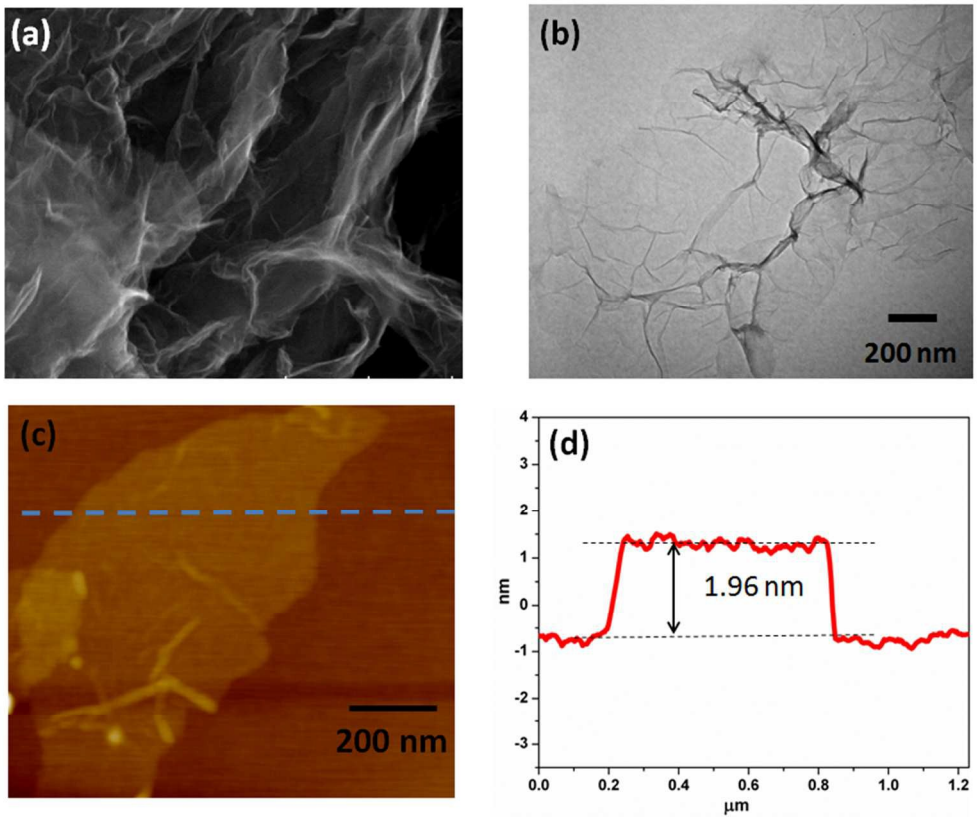

Fig. 1 (a) Cross-section SEM and (b) TEM images of the TEA/rGO composite; (c) AFM image of the individual TEA/rGO sheet with (d) a corresponding height profile showing the average thickness.

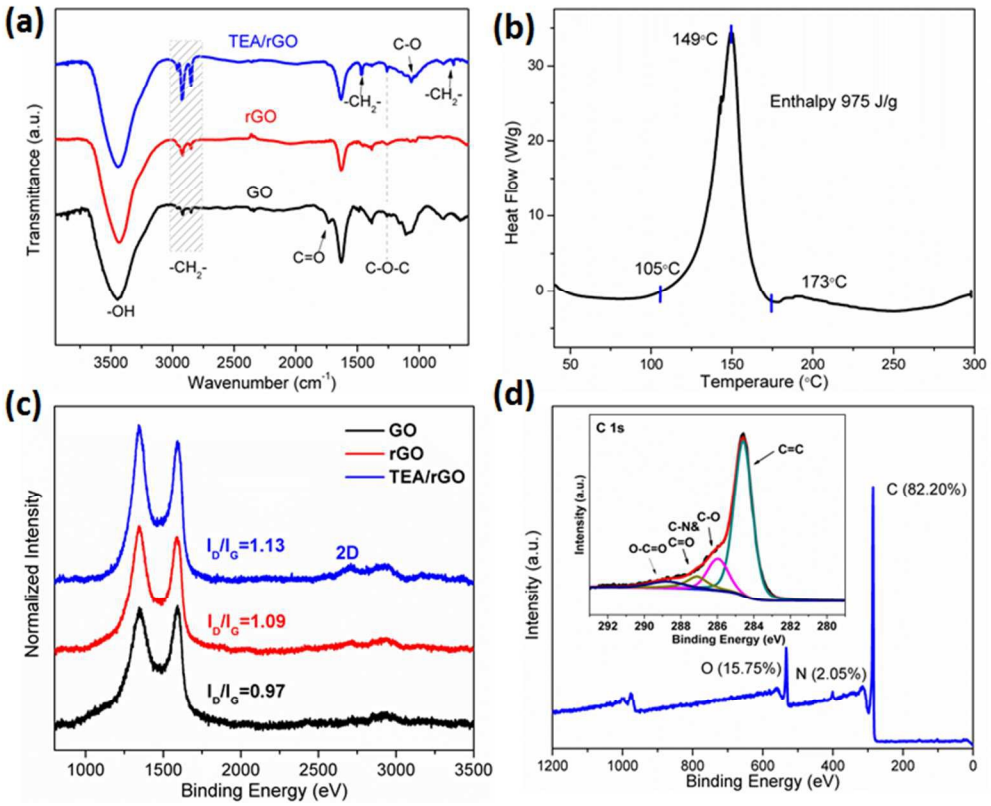

Fig. 2 (a) FTIR spectra and (c) Raman spectra of GO, rGO and TEA/rGO composites; (b) DSC curves of GO/TEA mixture in N_2 atmosphere with heating rate of 10°C/min; (d) survey and C1s (inset) spectra of TEA/rGO composite.

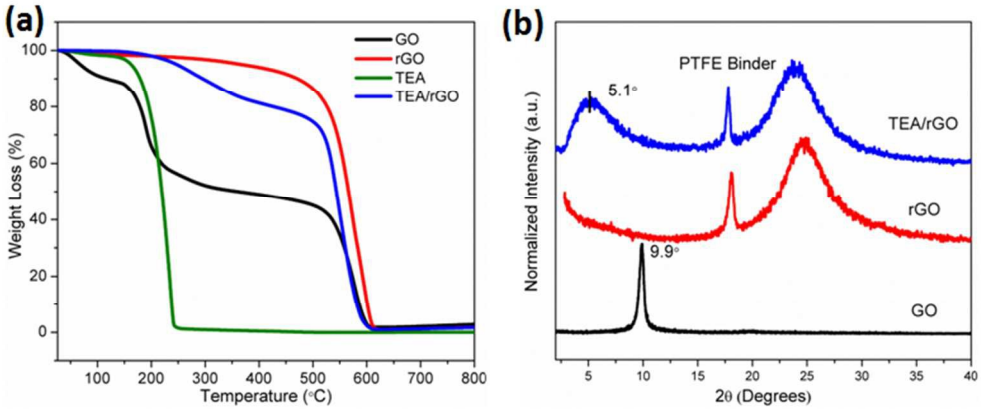

Fig 3(a) TGA curves of all samples and precursors in air at a heating rate of 10°C/min; (b) XRD patterns of GO, rGO and TEA/rGO.

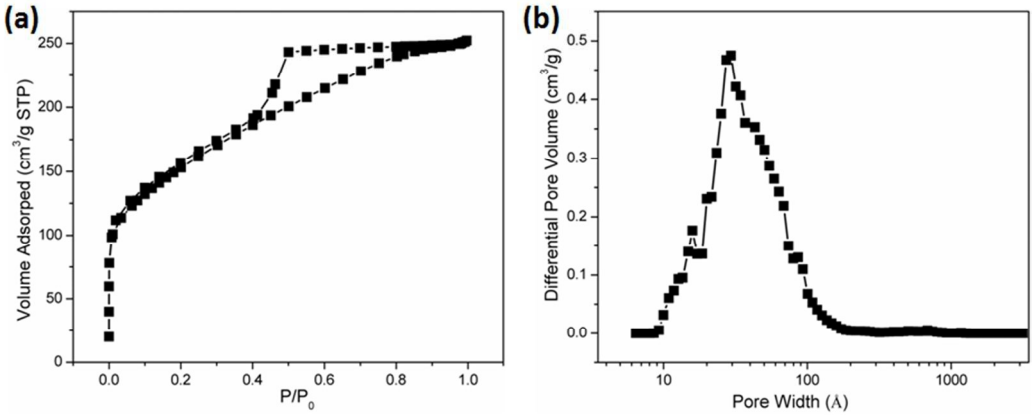

Fig. 4 (a) Nitrogen adsorption/desorption isotherm and (b) pore size distribution plots of TEA/rGO sample.

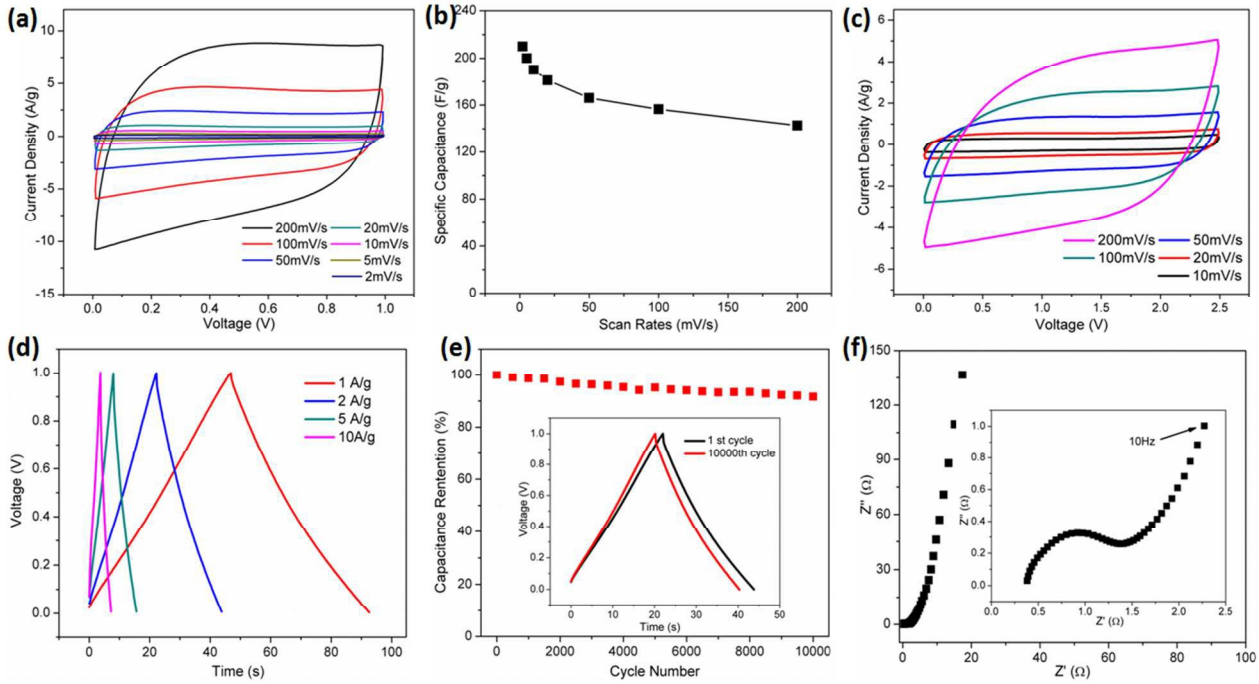

Fig. 5 Electrochemical properties of the as-fabricated electrode in two-electrode system. (a) CV curves of TEA/rGO in 1 M H_2SO_4 electrolyte at different scan rates; (b) rate-dependent plot of the specific capacitance values; (c) CV curves of the electrode tested in 1 M $TEABF_4$/AN; (d) galvanostatic CD curves of TEA/rGO at various current densities; (e) capacitance retention at 10,000 cycles at 2 A/g with first and 10000^{th} CD plots in the inset; (f) Nyquist plot of the TEA/rGO electrode with a magnified view at high-frequency region.

Graphical Abstract